

Showcasing research from DSc Piotr Garbacz's Nuclear Magnetic Resonance Laboratory, Faculty of Chemistry, University of Warsaw, Poland.

Direct enantiomeric discrimination through antisymmetric hyperfine coupling

This Communication shows that the antisymmetric hyperfine coupling ( $A^*$ ) in polar radicals is crucial for direct enantiomeric discrimination by EPR. The effect's sensitivity to chirality follows from the transformation of the  $A^*$  vector and the electric dipole under mirror reflection.

As featured in:



See Piotr Garbacz and Juha Vaara,  
*Chem. Commun.*, 2021, **57**, 8264.





Cite this: *Chem. Commun.*, 2021, 57, 8264

Received 17th May 2021,  
Accepted 23rd June 2021

DOI: 10.1039/d1cc02579a

rsc.li/chemcomm

# Direct enantiomeric discrimination through antisymmetric hyperfine coupling†‡

Piotr Garbacz \*<sup>a</sup> and Juha Vaara <sup>b</sup>

**Chiral open-shell molecules possessing permanent electric dipole moments have an EPR signal at the difference frequency of the electron and nuclear resonances, allowing direct enantiomeric discrimination by signal phase. The effect depends on the vector antisymmetry of the hyperfine coupling. Quantum chemistry suggests chiral bisfluorene methyl radical derivatives as promising for experiments.**

The hyperfine coupling (HFC) between the spins of an unpaired electron and a nucleus provides important information about the molecular structure and interactions.<sup>1,2</sup> However, the techniques used in electron paramagnetic resonance (EPR) spectroscopy can so far only indirectly be applied to distinguish the enantiomers of chiral molecules, *e.g.*, by transforming the molecule to a diastereoisomeric entity by chiral environment such as a gel or a chiral solvent, or by conducting a reaction with a chiral derivatizing agent.<sup>3,4</sup> In this letter we propose a new effect that allows direct chiral discrimination from the vector of antisymmetric HFC,  $\mathbf{A}^*$ . Typically the sensitivity of measurements of the electron spin transitions surpasses that of nuclear transitions by several orders of magnitude.<sup>5</sup> Thus, the effect caused by  $\mathbf{A}^*$  puts us in a good position to achieve direct sensitivity to chirality in EPR. Ref. 6–11 discuss other chirality-sensitive nuclear spin effects. An alternative possibility provided by the chiral-induced spin selectivity effect (CISS) is presented in ref. 12 and 13.

The spin Hamiltonian  $\mathcal{H}$  for an unpaired electron  $S$  interacting with a spin-1/2 nucleus  $I$ ,<sup>14</sup>

$$\mathcal{H} = \mathcal{H}_A + \mathcal{H}_B = \mathcal{H}_A + \mathcal{H}_S + \mathcal{H}_I, \quad (1)$$

includes the HFC of the corresponding spin operators  $\hat{S}$  and  $\hat{I}$ ,

$$\mathcal{H}_A = h\hat{S} \cdot \mathbf{A} \cdot \hat{I}, \quad (2)$$

and the Zeeman interactions with the magnetic field  $\mathbf{B}_0$ :

$$\mathcal{H}_S = -\mu_B \mathbf{B}_0 \cdot \mathbf{g}_S \cdot \hat{S}, \quad (3)$$

$$\mathcal{H}_I = -\mu_N \mathbf{B}_0 \cdot \mathbf{g}_I \cdot \hat{I}. \quad (4)$$

Here,  $\mathbf{A}$  (in MHz) is the HFC tensor, and  $\mathbf{g}_S$  and  $\mathbf{g}_I$  are the  $g$ -tensors of  $S$  and  $I$ . Overlooking the very small parity non-conservation effects,<sup>15</sup> eqn (1) holds for both enantiomers.

For a liquid sample of molecules with permanent electric dipole  $\mu_e$ , its isotropic average due to  $\mathcal{H}$  at temperature  $T$  is

$$\langle \mu_e^c \rangle = \frac{\int \mu_e \exp(-\mathcal{H}/(k_B T)) d\Omega}{\int \exp(-\mathcal{H}/(k_B T)) d\Omega} \approx -\langle \mu_e \mathcal{H} / (k_B T) \rangle_{\text{iso}}, \quad (5)$$

with  $\Omega$  denoting the molecular orientation and assuming that the eigenvalues of  $\mathcal{H}$  are small compared to  $k_B T$ , and hence,

$$\langle \mu_e^c \rangle = \langle \mu_e^{c,A} \rangle + \langle \mu_e^{c,B} \rangle, \quad (6)$$

$$\langle \mu_e^{c,A} \rangle = -h\mathbf{A}^c \cdot \hat{S} \times \hat{I}, \quad (7)$$

$$\langle \mu_e^{c,B} \rangle = (\mu_B g_S^c \hat{S} + \mu_N g_I^c \hat{I}) \times \mathbf{B}_0. \quad (8)$$

with the pseudoscalars

$$A^c = \frac{1}{6k_B T} \epsilon_{\alpha\beta\gamma} \mu_{e,\alpha} A_{\beta\gamma} = \frac{1}{3} \frac{\mu_e \cdot \mathbf{A}^*}{k_B T}, \quad (9)$$

$$g_S^c = \frac{1}{6k_B T} \epsilon_{\alpha\beta\gamma} \mu_{e,\alpha} g_{S,\beta\gamma} = \frac{1}{3} \frac{\mu_e \cdot \mathbf{g}_S^*}{k_B T}, \quad (10)$$

$$g_I^c = \frac{1}{6k_B T} \epsilon_{\alpha\beta\gamma} \mu_{e,\alpha} g_{I,\beta\gamma} = \frac{1}{3} \frac{\mu_e \cdot \mathbf{g}_I^*}{k_B T}. \quad (11)$$

The two-index tensors  $\mathbf{A}$ ,  $\mathbf{g}_S$ , and  $\mathbf{g}_I$  can be decomposed as the sums of three irreducible tensors: the rank-0 isotropic (*e.g.*,  $A^{\text{iso}}$ ), the rank-1 antisymmetric ( $\mathbf{A}^{\text{anti}}$ ) and the rank-2 (traceless) symmetric ( $\mathbf{A}^{\text{sym}}$ ) parts.<sup>16</sup> We have in eqn (9)–(11) expressed  $\mathbf{A}^{\text{anti}}$  as the vector  $\mathbf{A}^*$  whose components are  $(\mathbf{A}^*)_\alpha = \frac{1}{2} \epsilon_{\alpha\beta\gamma} A_{\beta\gamma}$ .

<sup>a</sup> Faculty of Chemistry, University of Warsaw, Pasteura 1, 02-093 Warsaw, Poland.  
E-mail: pgarbacz@chem.uw.edu.pl; Tel: +48-22-55-26-346

<sup>b</sup> NMR Research Unit, University of Oulu, P.O. Box 3000, FI-90014 Oulu, Finland.  
E-mail: juha.vaara@iki.fi

† This article is dedicated to the memory of Prof. A. D. Buckingham (1930–2021), whose theoretical research laid the foundation for the magnetic resonance spectroscopy of chiral molecules.

‡ Electronic supplementary information (ESI) available. See DOI: 10.1039/d1cc02579a



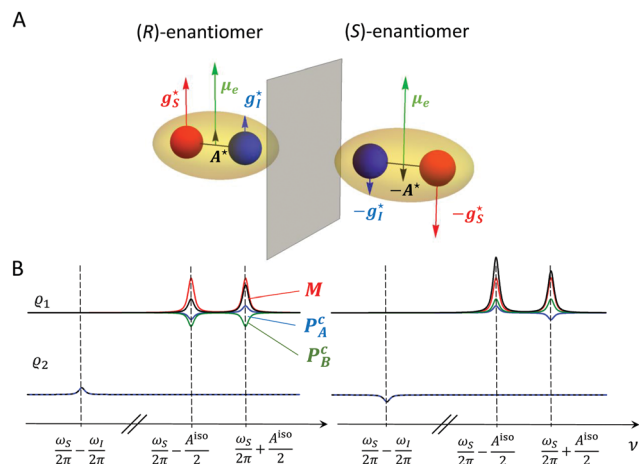


**Fig. 1** (A) Permanent electric dipole moment ( $\mu_e$ ) and the vector antisymmetries of the hyperfine coupling tensor ( $A^*$ ) and  $g$ -tensors of the electron and the spin-1/2 nucleus ( $g_S^*$  and  $g_I^*$ ) for a chiral molecule and its mirror image. (B) Expected signals of the enantiomers due to the precession of the magnetization ( $M$ , red color) and the oscillation of the chirality-sensitive electric polarization ( $P_A^c$ , blue, and  $P_B^c$ , green) for two different initial states of the spin system. The total signal shown in black.

While  $\mu_e$  is a polar vector,  $A^*$  is axial, since the part of the Hamiltonian  $\mathcal{H}_A$  relevant to  $A^*$  transforms under inversion as  $A^* \cdot (\hat{S} \times \hat{I}) \rightarrow (-A^*) \cdot \{ -[(-\hat{S}) \times (-\hat{I})] \}$ .<sup>17</sup> Therefore, the product  $\mu_e \cdot A^*$  changes its sign under mirror reflection of the molecule and, consequently, the pseudoscalar  $A^c$  has opposite signs for enantiomers. It follows that, in an achiral dipolar molecule,  $\mu_e \cdot A^* = 0$ , hence  $\mu_e$  and  $A^*$  are perpendicular to each other and  $A^c = 0$ . The same applies to the pseudoscalars  $g_S^c$  and  $g_I^c$  drawn from the  $g$ -tensors  $g_S$  and  $g_I$  (Fig. 1A).

When a sample is excited by electromagnetic field, the observed signal  $\mathcal{S}(t)$  arises from the electron and nuclear magnetization

$$M(t) = \text{Tr} \left[ \mathcal{N} \left( \mu_B g_S^{\text{iso}} \hat{S} + \mu_N g_I^{\text{iso}} \hat{I} \right) \hat{\rho}(t) \right] \quad (12)$$

and the chirality-sensitive electric polarization

$$P^c(t) = \text{Tr} \left[ \mathcal{N} \langle \mu_e^c \rangle \hat{\rho}(t) \right]. \quad (13)$$

Here,  $\mathcal{N}$  is the number density of the molecules and  $\hat{\rho}(t)$  is the density matrix of the spin system. The expected signal is proportional to the time derivative of the magnetization  $\frac{d}{dt}M(t) = \dot{M}(t)$  and the polarization  $\frac{d}{dt}P^c = \dot{P}^c(t)$  as

$$\mathcal{S}(\nu) \propto \int_V (\dot{M} \cdot B_1 + \dot{P}^c \cdot E_1) d\tau. \quad (14)$$

$B_1$  and  $E_1$  are the amplitude vectors of the magnetic and electric field, respectively, which can be generated by the detector at frequency  $\nu$ .<sup>18</sup> The integration is over the volume of the sample.

Assume  $B_0$  along the laboratory  $z$  axis. Due to the vector products in eqn (7) and (8), the observation of  $P^c$  is only possible for states whose spin vectors have a non-vanishing component perpendicular to  $B_0$  (e.g.,  $\hat{S}_y$ ) or possess mutually perpendicular components (e.g.,  $\hat{S}_y \hat{I}_x$ ).

The time-dependence of the density operator  $\hat{\rho}(t)$  is found by solving the Liouville–von Neumann equation

$$i\hbar \frac{d}{dt} \hat{\rho}(t) = [\hat{\mathcal{H}}, \hat{\rho}(t)], \quad (15)$$

with the appropriate initial condition  $\hat{\rho}(0)$ . At high field, the Hamiltonian [eqn (1)] can be approximated as

$$\hat{\mathcal{H}} \approx \hbar\omega_S \hat{S}_z + \hbar\omega_I \hat{I}_z + hA^{\text{iso}} \hat{S}_z \hat{I}_z, \quad (16)$$

where  $\hbar\omega_S = -\mu_B g_S^{\text{iso}} B_0$  and  $\hbar\omega_I = -\mu_N g_I^{\text{iso}} B_0$ .<sup>19</sup> Let us next consider two experiments beginning from the thermal equilibrium

$$\hat{\rho}_{\text{eq}} = \mathbf{1}/4 + \langle \hat{S}_z \rangle_{\text{eq}} \hat{S}_z + \langle \hat{I}_z \rangle_{\text{eq}} \hat{I}_z + \langle \hat{S}_z \hat{I}_z \rangle_{\text{eq}} \hat{S}_z \hat{I}_z, \quad (17)$$

where  $\langle \hat{S}_z \rangle_{\text{eq}} = -\hbar\omega_S/(4k_B T)$ ,  $\langle \hat{I}_z \rangle_{\text{eq}} = -\hbar\omega_I/(4k_B T)$ , and  $\langle \hat{S}_z \hat{I}_z \rangle_{\text{eq}} = -hA^{\text{iso}}/(4k_B T)$ .

**Case I.** A  $\left(\frac{\pi}{2}\right)_x$  pulse of the  $B_1$  field on  $\hat{\rho}_{\text{eq}}$  generates the state

$$\hat{\rho}_1(0) = -\langle \hat{S}_z \rangle_{\text{eq}} \hat{S}_y + \langle \hat{I}_z \rangle_{\text{eq}} \hat{I}_x - \langle \hat{S}_z \hat{I}_z \rangle_{\text{eq}} \hat{S}_y \hat{I}_x. \quad (18)$$

Solving eqn (15) one finds

$$\hat{\rho}_1(t) = [\cos(\pi A^{\text{iso}} t) \sin(\omega_S t) \hat{S}_x + \sin(\pi A^{\text{iso}} t) \cos(\omega_S t) \hat{S}_x \hat{I}_z] \langle \hat{S}_z \rangle_{\text{eq}} + \dots \quad (19)$$

with the detection defined by  $B_1 = B_1 e_x$  and  $E_1 = E_1 e_y$ ,  $M_x$  and  $P_y^c$  in eqn (12) and (13) may contribute to the signal. In eqn (19), both terms that (i) do not contribute to  $\mathcal{S}(\nu)$  and/or (ii) are much smaller than  $\langle \hat{S}_z \rangle_{\text{eq}}$ , i.e., proportional to  $\langle \hat{S}_z \hat{I}_z \rangle_{\text{eq}}$ , are omitted. Then, the expected signal is

$$\begin{aligned} \mathcal{S}_1 \left( \frac{\omega_S}{2\pi} \pm \frac{A^{\text{iso}}}{2} \right) &\propto \mathcal{N} \left( \frac{\omega_S}{2\pi} \pm \frac{A^{\text{iso}}}{2} \right) \\ &\times \left[ \mu_B g_S^{\text{iso}} B_1 + \left( -\mu_B g_S^c B_0 \pm \frac{1}{2} h A^c \right) E_1 \right] \langle \hat{S}_z \rangle_{\text{eq}}. \end{aligned} \quad (20)$$

The signals of  $P^c$  appear at the same frequencies as  $M$ , forcing discrimination between the two require the measurement of the amplitude difference of the components of the EPR doublet (Fig. 1B, the first spectrum).

**Case II.** For a different initial spin state

$$\hat{\rho}_2(0) = -\langle \hat{S}_z \rangle_{\text{eq}} \hat{S}_y \hat{I}_x + \langle \hat{I}_z \rangle_{\text{eq}} \hat{I}_x - \langle \hat{S}_z \hat{I}_z \rangle_{\text{eq}} \hat{S}_y, \quad (21)$$

which can be obtained by applying the pulse sequence  $\left(\frac{\pi}{2}\right)_{-y}^S - \left(\frac{1}{2A^{\text{iso}}}\right) - \left(\frac{\pi}{2}\right)_y^I$  on  $\hat{\rho}_{\text{eq}}$ , one finds the density matrix

$$\hat{\rho}_2(t) = \frac{1}{2} \cos[(\omega_S - \omega_I)t] (\hat{S}_x \hat{I}_y - \hat{S}_y \hat{I}_x) \langle \hat{S}_z \rangle_0 + \dots \quad (22)$$

If the electric field detection is changed into  $E_1 = E_1 e_z$ , the signal becomes

$$\mathcal{S}_2 \left( \frac{\omega_S}{2\pi} - \frac{\omega_I}{2\pi} \right) \propto \mathcal{N} \left( \frac{\omega_S}{2\pi} - \frac{\omega_I}{2\pi} \right) h A^c E_1 \langle \hat{S}_z \rangle_{\text{eq}}. \quad (23)$$

$\hat{\rho}_2(t)$  only generates signal of the chirality-sensitive  $P_A^c$  at the difference frequency  $\omega_S - \omega_I$ . This allows to distinguish the postulated chirality-sensitive effect from other, nonchiral



effects.  $\mathbf{P}_A^c$  has the same direction as  $\mathbf{B}_0$  (Fig. 1B, the second spectrum).

The phases and amplitudes of  $\mathbf{B}_1$  and  $\mathbf{E}_1$  depend on the particular experimental implementation (see ref. 20 for examples). If the electronic relaxation time is long in comparison with the  $(\pi/2)_y^I$  pulse, one can presume that the case II, *i.e.*,  $\hat{\rho}_2(0) \propto \hat{S}_y \hat{I}_x$ , represents a promising initial state. Spin relaxation toward the thermodynamic equilibrium causes  $\hat{S}_z$  and  $\hat{I}_z$  to appear. However, being parallel to  $\mathbf{B}_0$ , they do not generate any observable signals. One can hypothesize the inverse effect to that described above, *i.e.*, that excitation by oscillating electric field would cause changes of the spin state that are dependent on the molecular chirality. Observing the inverse effect would be, however, complicated by dielectric heating since, due to the smallness of chirality-sensitive effects, an electric field of high amplitude is required.

We study neutral organic radicals depicted in Fig. 2: nitroxyls, *i.e.*, 2,2,6,6-tetramethyl-1-piperidinyloxy (**1a**; TEMPO), the TEMPO derivative of (*R*)-alanine [(*R*)-**1b**], 1,3,5-trimethyl-6-oxoverdazyl (**2a**), and the verdazyl derivative of (*R*)-phenylalanine [(*R*)-**2b**], as well as carbon-centered radicals: triphenylmethyl (**3a**), bis(fluoren-9-yl)methyl (**3b**), and bisfluorene methyl derivative of (*R*)-alanine [(*R*)-**3c**]. **3a** and **3b**, whose rigid structures are non-superposable on their mirror images, do not exhibit chiral properties due to fast interconversion of their enantiomers. Chiral samples are **1b**, **2b**, and **3c**.

The molecular structures were computationally optimized as described in ESI†. The  $\mathbf{A}$  tensors were calculated using unrestricted density-functional theory (DFT) at the fully relativistic matrix-Dirac-Kohn-Sham (mDKS) level<sup>21,22</sup> on the ReSpect code,<sup>23,24</sup> using mainly the PBE0 hybrid functional<sup>25</sup> and the pcH-2 large-component basis sets of ref. 26. See ESI† for further details. The results of computed eigenvalues of  $\mathbf{A}$  are in a reasonable agreement with literature (Table S9 in the ESI†). The experiments have been at various temperatures and physical states, whereas the computations were performed for single molecules at the equilibrium geometry *in vacuo*. However, such differences can easily be masked by the dependence of  $\mathbf{A}$  on the chosen functional.<sup>27,28</sup>

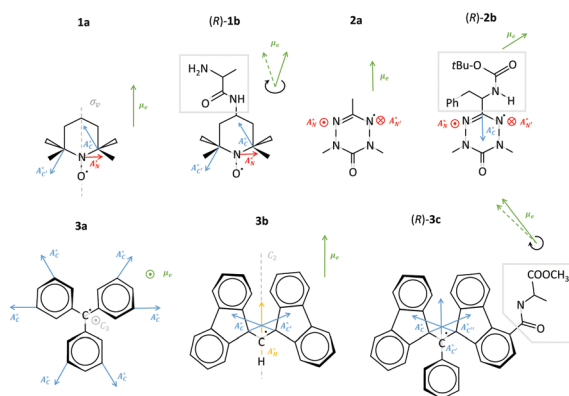


Fig. 2 Antisymmetric parts of the hyperfine coupling tensors  $\mathbf{A}^*$  and permanent electric dipole moments  $\mu_e$  of the studied radicals.

Table 1 Permanent electric dipole moment  $\mu_e$  (D), the isotropic part  $A_{\text{iso}}$  (MHz) and the length of antisymmetry vector,  $A^*$  (kHz), of the hyperfine coupling tensor, and the pseudoscalar  $A^c$  ( $\mu\text{Hz m V}^{-1}$ ).  $A^c$  is only listed for chiral species whose enantiomers do not interconvert in solution

Radical	$\mu_e$	Nucleus/position	$A_{\text{iso}}$	$A^*$	$A^c$
<b>1a</b>	3.03	$^{15}\text{N}$	−51.3	161.8	
		$^{13}\text{CNO}^\bullet$	−9.4	203.8	
( <i>R</i> )- <b>syn-1b</b>	4.85	$^{15}\text{N}$	−51.4	166.9	−30.5
		$^{13}\text{CNO}^\bullet$	−9.6	199.9	27.3
( <i>R</i> )- <b>anti-1b</b>	4.80	$^{15}\text{N}$	−51.6	166.9	49.4
		$^{13}\text{CNO}^\bullet$	−9.5	200.2	−31.5
<b>2a</b>	1.12	$^{15}\text{N}$	−22.6	46.4	
( <i>R</i> )- <b>2b</b>	2.23	$^{15}\text{N}$	−22.6	49.5	2.3
		$^{13}\text{C}$	−32.5	21.9	−8.3
<b>3a</b>	0.000193	$^{13}\text{C}$	−11.2	9.8	
<b>3b</b>	0.0375	$^{13}\text{CC}^\bullet\text{H}$	40.7	12.2	
		$\text{CC}^\bullet\text{H}$	42.8	23.3	
( <i>R</i> )- <b>3c</b>	2.69	$^{13}\text{CC}^\bullet\text{C}$	43.3	13.5	−6.4
		$\text{C}^{13}\text{C}^\bullet\text{C}$	−40.7	11.3	4.4
		$\text{CC}^{13}\text{C}^\bullet\text{C}$	43.7	15.9	6.9

In contrast to the antisymmetry  $g_s^*$  of the electronic  $g$ -tensor, which is a few times larger than the nuclear  $g^*$  (Tables S10 and S11 in ESI† and ref. 29, 30), the antisymmetry  $A^*$  of the HFC tensor is larger by about three orders of magnitude than the antisymmetric part of the indirect spin-spin coupling tensor in diamagnetic molecules.<sup>31</sup> The direction of  $A^*$  and its magnitude are mainly determined by the local electronic structure of the molecule and vary weakly when a chiral substituent is placed in a distal position with respect to the maximum of the unpaired electron density (Table 1; all components of HFC tensors and dipole moments are given in Tables S12–S20 of the ESI†). *E.g.*,  $A_N^*$  of the nitroxyl nitrogen and  $A_C^*$  of the adjacent carbons differ by less than 1% in **1a** and (*R*)-**1b**. Similarly, the antisymmetries  $A_N^*$  of radicals **2a** and (*R*)-**2b** are almost unaffected by the chiral amino acid substituent.

Chiral substituent may noticeably change the permanent electric dipole  $\mu_e$ . For an achiral molecule,  $\mu_e$  is perpendicular to  $A^*$  [eqn (9)]. The sum of the scalar products  $\mu_e \cdot A^*$  of two equivalent nuclei may vanish also in a chiral system. *E.g.*, in **1a** (Fig. 2),  $\mu_e$  is in the  $\sigma_v$  plane of the molecule, whereas  $A_N^*$  of the nitroxyl nitrogen is perpendicular to that plane. While the  $A_C^*$  and  $A_{C'}^*$  of the adjacent carbons are not perpendicular to the  $\sigma_v$  plane, their projections onto this plane cancel, and the overall chirality-sensitive effect vanishes. However, if the molecule were isotopically  $^{13}\text{C}$ -labeled at the C position with  $^{12}\text{C}$  at the C' position, **1a** would be chiral and the predicted effect might be observed.

To maximize  $A^c$ , one has to orient the chiral substituent such that  $\mu_e$  is maximally parallel to  $A^*$ . For (*R*)-**1b**, the (*R*)-alanine substituent is placed at the opposite site to the nitroxyl group and its presence causes a tilt of  $\mu_e$ . However, (*R*)-**1b** has two dominating conformers: *syn* with the carbonyl oxygen atom nearby the  $\text{CH}_3$  group and *anti*, where the CO and  $\text{CH}_3$  groups are distant (Fig. S1 in ESI†). The dipole moments  $\mu_e$  of the two conformers are oppositely tilted, thus  $A_{N,\text{syn}}^c \approx -A_{N,\text{anti}}^c$  and the chirality-sensitive effect is greatly suppressed. While  $A_C^c$  and  $A_{C'}^c$  cancel out entirely for the isotopically unsubstituted molecule (*vide supra*), the effect of the substitution on  $A_C^{\text{iso}}$  is of the order





of a fraction of MHz and, therefore, the chiral signal would presumably average to almost zero. A similar result is obtained for the nitrogen atoms of (*R*)-**2b**.

Comparison of **3a** and **3b** with (*R*)-**3c** shows that the carbon-centered radicals require a chiral substituent that ensures a sufficiently large  $\mu_c$ .  $A_C^*$  of **3b** is only weakly affected by the (*R*)-alanine group but, due to more favorable orientation of  $\mu_c$  with respect to  $A_C^*$ ,  $A_C^c$  reaches a much higher amplitude of 10–15 kHz. In this case, the amplitude of the expected chiral effect is at least 5 nHz m V<sup>-1</sup>, meaning that its detection by the equipment currently used in electron-nucleus double resonance experiments is feasible. When X-band ( $\frac{\omega_C}{2\pi} \approx 3.2$  MHz) or W-band ( $\frac{\omega_C}{2\pi} \approx 36$  MHz) EPR is applied, the signal of  $P_A^c$  will not overlap with any residual standard EPR signal, which could be present due to the finite purity of the desired initial state, i.e.,  $-S_y I_x$ .

A further advantage of the **3c** over **1b** or **2b** is the more efficient generation of the initial spin state, since the expected relaxation time of **3c** is approx. 10  $\mu$ s based on  $T_2$  for an unsubstituted **3c**.<sup>32</sup> This is comparable with the length of the  $\pi/2$  pulse, whereas the typical TEMPO relaxation time does not exceed several dozen ns. Assuming that the ratio between the electric and magnetic fields of the detector is  $cB_1/E_1 = 10^3$  and selectively <sup>13</sup>C-enriched **3c**, one finds that the amplitude of the expected chirality-sensitive signal of  $P_A^c$  is of the order of  $10^{-4}$  of the standard EPR signal.

To conclude, it is predicted that with a suitably chosen initial spin state, the electron-nucleus system generates an electric polarization  $P^c$  whose phase directly identifies the handedness of the molecule.  $P^c$  oscillates at the difference frequency of the electron and nuclear resonances in the direction of the main, static magnetic field. Largest magnitude of the effect is obtained if the permanent electric dipole and the antisymmetric HFC tensor, represented as a vector, are parallel to each other. This condition is fulfilled by a chiral derivative of bisfluorene **3c**, which is a good candidate for forthcoming experiments. We believe that the predicted effect has potential for EPR investigations of chiral systems.

PG acknowledges the National Science Centre, Poland, for the financial support through OPUS 16 Grant No. 2018/31/B/ST4/02570 and Bartosz Kreft (U. Warsaw) for his help in computations. JV has received funding from the Academy of Finland (grant 331008) and U. Oulu (Kvantum Institute). Computations were carried at CSC-the Finnish IT Centre for Science and the Finnish Grid and Cloud Infrastructure project (persistent identifier urn:nbn:fi:research-infras-2016072533).

## Note added after first publication

This article replaces the version published on 29th July 2021, which contained errors in eqn (2), (3), (4), (7), (8) and (9).

## Conflicts of interest

There are no conflicts to declare.

## Notes and references

- 1 K. Möbius, W. Lubitz, N. Cox and A. Savitsky, *Magnetochemistry*, 2018, **4**, 50.
- 2 M. M. Roessler and E. Salvadori, *Chem. Soc. Rev.*, 2018, **47**, 2534–2553.
- 3 H. B. Stegmann, H. Wendel, H. Dao-Ba, P. Schuler and K. Scheffer, *Angew. Chem., Int. Ed. Engl.*, 1986, **25**, 1007–1008.
- 4 C. D. Stevenson, A. L. Wilham and E. C. Brown, *J. Phys. Chem. A*, 1998, **102**, 2999–3001.
- 5 G. A. Rinard, R. W. Quine, S. S. Eaton and G. R. Eaton, in *Frequency Dependence of EPR Sensitivity*, ed. L. J. Berliner and C. J. Bender, Springer US, Boston, MA, 2004, p. 118.
- 6 P. Garbacz and A. D. Buckingham, *J. Chem. Phys.*, 2016, **145**, 204201.
- 7 A. D. Buckingham, *J. Chem. Phys.*, 2014, **140**, 011103.
- 8 P. Garbacz, *J. Chem. Phys.*, 2016, **145**, 224202.
- 9 J. P. King, T. F. Sjolander and J. W. Blanchard, *J. Phys. Chem. Lett.*, 2017, **8**, 710–714.
- 10 A. Soncini and S. Calvello, *Phys. Rev. Lett.*, 2016, **116**, 163001.
- 11 S. Calvello and A. Soncini, *Phys. Chem. Chem. Phys.*, 2020, **22**, 8427–8441.
- 12 R. Naaman, Y. Paltiel and D. Waldeck, *Nat. Rev. Chem.*, 2019, **3**, 250–260.
- 13 R. Naaman and D. Waldeck, *Annu. Rev. Phys. Chem.*, 2015, **66**, 263–281.
- 14 A. Schweiger and G. Jeschke, *Principles of pulse electron paramagnetic resonance*, Oxford University Press, Oxford, 2001, p. 29.
- 15 A. L. Barra and J. B. Robert, *Mol. Phys.*, 1996, **88**, 875–886.
- 16 D. A. Varshalovich, A. N. Moskalev and V. K. Khersonskii, *Quantum Theory of Angular Momentum*, World Scientific, 1989, p. 63.
- 17 We found by quantum-chemical computations that the relation  $A^{*'} = \det(R)RA^*$  of the pseudovector transformation holds ( $R$  is a rotation matrix of radical coordinates). Thus, the coupling of the electron spin with molecular rotation may be neglected.
- 18 The signal depends on the sensitivity of the detector to the excitation by  $\vec{M}$  and  $\vec{P}^c$ . According to the reciprocity theorem, the sensitivity is proportional to the magnitude of the field that the detector would generate if voltage of the same amplitude as observed would be used for exciting the detector.
- 19 For an electron,  $g_S < 0$ , thus the angular frequency  $\omega_S > 0$  and the spin  $S$  precesses anticlockwise according to the right-hand rule. The reverse is true for a nucleus with  $g_I > 0$  (such as <sup>1</sup>H and <sup>13</sup>C); in this case the angular frequency  $\omega_I < 0$ , i.e., the spin  $I$  precesses clockwise.
- 20 E. Reijerse and A. Savitsky, *EPR Spectroscopy: Fundamentals and Methods*, Wiley, 2018, pp. 242–251.
- 21 E. Malkin, M. Repický, S. Komorovský, P. Mach, O. Malkina and V. G. Malkin, *J. Chem. Phys.*, 2011, **134**, 044111.
- 22 S. Gohr, P. Hrobárik, M. Repický, S. Komorovský, K. Ruud and M. Kaupp, *J. Phys. Chem. A*, 2015, **119**, 12892–12905.
- 23 M. Repický, S. Komorovský, M. Kadek, U. Konecny, L. Ekström, E. Malkin, M. Kaupp, K. Ruud, O. L. Malkina and V. G. Malkin, *J. Chem. Phys.*, 2020, **152**, 184101.
- 24 M. Repický, S. Komorovský, V. G. Malkin, O. L. Malkina, M. Kaupp and K. Ruud, ReSpec, version 5.1.0 (2019); Relativistic Spectroscopy DFT program, with contributions from R. Bast, U. Ekström, M. Kadek, S. Knecht, L. Konecny, E. Malkin and I. Malkin-Ondik. See <http://www.respectprogram.org>.
- 25 C. Adamo and V. Barone, *J. Chem. Phys.*, 1999, **110**, 6158–6170.
- 26 P. Jakobsen and F. Jensen, *J. Chem. Phys.*, 2019, **151**, 174107.
- 27 M. Bühl, *Chem. Phys. Lett.*, 1997, **267**, 251–257.
- 28 J. Vaara, *Phys. Chem. Chem. Phys.*, 2007, **9**, 5399–5418.
- 29 P. Garbacz, J. Cukras and M. Jaszuński, *Phys. Chem. Chem. Phys.*, 2015, **17**, 22642–22651.
- 30 A. D. Buckingham, P. Lazzeretti and S. Pelloni, *Mol. Phys.*, 2015, **113**, 1780–1785.
- 31 P. Garbacz, *Mol. Phys.*, 2018, **116**, 1397–1408.
- 32 V. Meyer, S. S. Eaton and G. R. Eaton, *Appl. Magn. Reson.*, 2014, **45**, 993–1007.

